Acta Materialia 188 (2020) 23–29

Contents lists available at ScienceDirect

Acta Materialia

journal homepage: www.elsevier.com/locate/actamat

Full length article

Atomic-Scale insight into the reversibility of polar order in ultrathin epitaxial Nb:$SrTiO_3$/$BaTiO_3$ heterostructure and its implication to resistive switching

Junxiang Yao[a,1], Mao Ye[b,1], Yuanwei Sun[c,d], Ye Yuan[e], Hua Fan[f], Yuan Zhang[g], Chao Chen[h], Cong Liu[a], Ke Qu[a], Gaokuo Zhong[a], Tingting Jia[a], Zhen Fan[h], Shanming Ke[i], Yue Zhao[f], Chungang Duan[e], Peng Gao[c,d], Jiangyu Li[a,*]

[a] Shenzhen Key Laboratory of Nanobiomechanics, Shenzhen Institutes of Advanced Technology, Chinese Academy of Sciences, Shenzhen, Guangdong 518055, China
[b] Department of Physics, Southern University of Science and Technology, Nanshan District, Shenzhen, 518055, Guangdong, China
[c] International Center for Quantum Materials, Peking University, Beijing 100871, China
[d] Electron Microscopy Laboratory, School of Physics, Peking University, Beijing 100871, China
[e] Key Laboratory of Polar Materials and Devices, Ministry of Education, East China Normal University, Shanghai 200062, China
[f] Institute for Quantum Science and Engineering and Department of Physics, South University of Science and Technology of China, Shenzhen 518055, China
[g] School of Materials Science and Engineering, Xiangtan University, Hunan 411105, China
[h] Institute for Advanced Materials and Guangdong Provincial Key Laboratory of Quantum Engineering and Quantum Materials, South China Academy of Advanced Optoelectronics, South China Normal University, Guangzhou 510006, China
[i] School of Materials Science and Engineering, Nanchang University, Nanchang 330031, China

ARTICLE INFO

Article History:
Received 1 October 2019
Revised 19 January 2020
Accepted 2 February 2020
Available online 5 February 2020

Keywords:
Ultrathin epitaxial ferroelectric semiconductor heterostructures
$BaTiO_3$/Nb:$SrTiO_3$
Resistive switching
Piezoresponse force microscopy
Atomic-scale polar order of ferroelectricity

ABSTRACT

Ferroelectric heterostructures with bi-stable state of polarization are appealing for data storage as well as tunable functionalities such as memristor behavior. While an increasing number of experimental and theoretical studies suggest that polarization persists in ultrathin epitaxial heterostructures approaching just a couple of unit cells, the switching of such polar order is much less well understood, and whether polarization can be reversed in ultrathin ferroelectric heterostructures remains to be answered. Here we fabricate high-quality 7-unit cell thick $BaTiO_3$ (BTO) films on Nb-doped single crystalline $SrTiO_3$ (NSTO) substrate, and demonstrate their apparent yet unambiguously false polarization reversal due to charge injection using comprehensive piezoresponse force microscopy (PFM) studies. The presence of weak polar order consistent with linear piezoelectricity is confirmed at the atomic scale by high resolution integrated differential phase contrast (IDPC) of scanning transmission electron microscopy (STEM) as well as macroscopic second harmonic generation (SHG), while the lack of polarization reversal under the voltage applied is supported by density functional theory calculation showing the persistence of dead layer on the surface. Nevertheless, poling-induced electric conduction differing by two orders of magnitude is observed, demonstrating resistive switching in ferroelectric heterostructure in the absence of polarization reversal, even with weak polar order. Our finding has technological implications on emerging memristor applications with potentially more accessible states than bi-stable polarization modulated mechanism, and raises technical challenges to unambiguously demonstrate polarization switching in ultrathin films at their critical size limit.

1. Introduction

Polarization is a long-range dipolar order that is spontaneously formed in crystalline solids, underpinning a variety of technologically important phenomena including piezoelectric coupling, pyroelectricity, nonlinear optic effect, and ferroelectric switching [1,2]. While many believed not long ago that there exists a relatively large critical size below which spontaneous polarization is suppressed [3,4], advances in film deposition has continuously pushed this limit down, and an increasing number of experimental and theoretical studies suggest that polarization persists in thin epitaxial films approaching just a couple of unit cells (u.c.). For example, $BaTiO_3$ (BTO) films were shown to possess polar order down to 3.5 u.c. in 2017 and 2 u.c. in 2019 [5,6], reaching and then overcoming its theoretical size limit predicted by density functional theory (DFT) in 2006 [7]. For PZT, it was reported in 2017 that polarization is significantly suppressed in

* Corresponding author.
E-mail address: jy.li1@siat.ac.cn (J. Li).
[1] These authors contribute equally to this work.

https://doi.org/10.1016/j.actamat.2020.02.001
1359-6454/

films less than 10 u.c., though it never vanished, suggesting the lack of critical thickness in PZT [8]. Similar phenomenon was also reported in $BiFeO_3$ (BFO), where polarization was found to persist in 1 u.c. film [9], and even in free-standing form [10]. These set of studies unambiguously establish polar order in the ultimate two-dimensional limit of epitaxial films, though the switching of such polar order is much less well understood.

Ferroelectric switching refers to polarization reversal under an external electric field, making it possible to access bi-stable states of polarization for data storage as well as tunable functionalities, for example resistive switching, memristor behavior, and ferroelectrically tuned magnetic skyrmions [11–13]. While ferroelectricity is conventionally characterized by polarization-electric field hysteresis loop measured at the macroscopic scale, large leakage current and small breakdown voltage often make such measurement virtually impossible in ultrathin films. Therefore, vast majority of works rely on piezoresponse force microscopy (PFM) to assess possible polarization switching at the nanoscale, with one notable exception using electron holography to infer ferroelectric switching in 5 nm particle of BTO [14]. It is now well known that PFM is prone to the interference of artifacts, particularly charge injections [2,15–17], which could lead to apparent yet false contrast in piezoresponse phase that is often used as a signature for polarization reversal. As a result, while polar orders in the ultrathin epitaxial films are well established, the practical capability to access their bi-stable polar state, and the implication to their tunable functionalities, remains to be examined. In other words, we do not know yet whether the polar order in ultrathin ferroelectrics approaching their critical size can be switched or not.

The question on polarization reversal is particularly important for ultrathin ferroelectric heterostructures that show interesting resistive switching behavior. For example, giant tunnel electroresistance effect in ultrathin BTO films was reported by a couple of groups in 2009 [18,19], correlating piezoresponse and local current measured by atomic force microscopy (AFM) at the nanoscale. On/off conductance ratio over 10^4 was then realized in $Pt/BaTiO_3/Nb:SrTiO_3$ heterostructure [20], in which BTO is 7 u.c. thick, and tunneling electroresistance was also reported in 1 u.c. BFO film [9]. These electroresistance effects have been attributed to polarization modulated barrier height and width, and thus the capability to switch and access the bi-stable polarization is critical. Nevertheless, it has been shown that electronic reconstruction at terrace edge of ultrathin BTO film also results in enhanced tunneling conduction [21], while light and voltage were found to modulate barrier height and width of 3 nm $Sm_{0.1}Bi_{0.9}FeO_3$ film as well [22]. These studies raise important questions on whether polarization can be reversed in ultrathin ferroelectric heterostructures, especially those approaching a few u.c., and if polarization reversal is prerequisite for resistive switching. Our study suggests that the answers to both questions are no.

Here we fabricate high quality 7 u.c. BTO films on Nb-doped single crystalline $SrTiO_3$ (NSTO) to study its polar order and polarization switching. While ordinary PFM characterization suggests linear piezoelectricity as well as apparent polarization reversal under electric poling, careful examination reveals that there is an absence of ferroelectric switching under the practically applied electric bias, where the apparent PFM phase contrast is resulted from charging injection, which is unstable and can be eliminated by grounding. The existence of weak polar order consistent with linear piezoelectricity is confirmed at the atomic scale by high resolution integrated differential phase contrast (IDPC) of scanning transmission electron microscopy (STEM) [8,14,23,24] as well as at macroscopic scale by the optic second harmonic generation (SHG) [25,26], while the lack of polarization reversal under the voltage applied is supported by density functional theory calculations showing the persistence of dead layer on the surface. Nevertheless, poling-induced electric conduction differing by two orders of magnitude is observed, demonstrating that polarization reversal is not necessary for resisting switching in ferroelectric heterostructures.

2. Experimental materials and methods

2.1. Sample fabrication

7 u.c. BTO ultra-thin films were deposited on 0.5 wt% NSTO (001) substrates by Laser Molecular Beam Epitaxial system (L-MBE) (PASCAL, KrF laser, λ = 248 nm). Before deposition, NSTO substrates were etched by buffered hydrofluoric acid for 30 s and then annealed at 900 °C for 2 h in air to create atomically smooth TiO_2-terminated surfaces with one-unit-cell height step. During the deposition, the temperature of the substrate was maintained at 700 °C with an oxygen partial pressure of 5 mTorr. After the deposition, the samples were cooled down to room temperature in the oxygen atmosphere at 1 atm with 20 °C/min. Then, Pt top electrodes (diameter = 50 μm) were fabricated by an E-beam evaporation (DE400, DE technology) at rate of 0.4 Å/s (120 mA 9.5 kW) in vacuum about 10^{-7} Torr.

2.2. Structure and property characterizations

Crystal structure of the ultra-thin BTO films was measured by X-ray diffraction (XRD) and reciprocal space mapping (RSM) using a SmartLab XRD with Cu *Kα* radiation (Rigaku, Japan). The growth process was monitored by *in situ* reflection high energy electron diffraction (RHEED), which shows the BTO layers are grown in a layer-by-layer mode.

For high-angle annular-dark-field (HAADF) and IDPC images acquisition, the cross-sectional STEM specimen was thinned to less than 30 μm first by using mechanical polishing and then we performed argon ion milling. The ion-beam milling was carried out using PIPSTM (Model 691, Gatan Inc.) with the accelerating voltage of 3.5 kV until a hole is made. In the following conditions, the guns were set at 1 keV for 2 mins with the angles of 3° and −3° for final surface cleaning. HAADF and IDPC images were recorded at 300 kV using an aberration-corrected FEI Titan Themis G2 with spatial resolutions up to 60 pm. The convergence semi-angle for imaging is 30 mrad, the collection semi-angles snap is 4 to 21 mrad for the IDPC imaging and 39 to 200 mrad for the HAADF.

The PFM mappings were conducted on atomic force microscopy (Asylum Cypher) under single frequency and commercial dual frequency resonant tracking (DART) modes, accompanying with *in situ* KPFM monitoring subsequently as time varies, using conductive tips (Nanoworld, EFM). Significant d_{33} loops were measured in DART mode, with reading *ac* voltage 800 mV and driving triangle-square waveforms. The special 1st and 2nd response measurements were performed statistically and computationally in single frequency mode by intentional programming, to visualize and tell the intrinsic piezoresponse and other artifacts. To be mentioned, 1st and 2nd response were collected with equivalent frequency around ω, while the ac excitations lie on ω and $\omega/2$ respectively [27]. Then, ORCA module was utilized to map conductive distributions and probe local I-V curves, both in BTO/NSTO heterostructures and bare NSTO monocrystalline substrates. Macroscopic high (low) resistive state was toggled and probed non-destructively based on the EVERBEING/BD-6 probe station equipped with a Keithley 2400 SourceMeter. All measurements are well grounded by connecting the bottom to the grounding lead.

The measurements of SHG are completed with a Ti:sapphire pulsed laser (laser amplifier system, 150 fs, 10 nJ, 76 MHz) in reflection configuration with an incident angle of 45. The 800 nm laser is used as incident fundamental beam. The sample is installed along the substrate of NSTO [100] direction, and no SHG signal was detected from substrates at the same incident power of the films. The measurements are made by rotating the polarization angle φ of the incident fundamental beam through a half-wave plate, and the *p*-polarized and *s*-polarized SHG signals are analyzed by Glan prisms. The polarization angle of φ = 0° or 180° is *p* polarization (p_{in}), while

the angle of φ = 90° or 270° are *s* polarization (s_{in}), respectively. The conversion SHG is achieved through the creation of a nonlinear polarization $P_i^{2\omega} \propto d_{ijk}E_jE_k$, where the d_{ijk} is the nonlinear optical coefficient tensor. As the tetragonal BTO films only have out-of-plane domain with the polarization direction perpendicular to the substrates, the generated *p*-polarized and *s*-polarized SHG signals are satisfied with the formula of $I_p \propto [A\cos(\varphi)^2 + B\sin(\varphi)^2]^2$ and $I_s \propto (C\sin(2\varphi))^2$, respectively [26]. From Fig. 3(c) and (d), we can found that the fitted results are compatible.

2.3. Theoretical simulation

The first-principles calculations were carried out based on the Vienna ab initio Simulation Package (VASP) within the generalized gradient approximation (GGA) of Perdew, Burke, and Ernzerhof (PBE) [41,42]. The energy cut-off is 450 eV for the plane wave basis set within ion cores modeled with projector augmented wave (PAW) potentials [41,42]. A vacuum region with a height of 20 Å was set in 10STO/mBTO (*m* = 3, 7, 10) structures and a well-converged 6 × 6 × 1 k-point mesh of the Monkhorst–Pack scheme was adopted for self-consistent calculations. In the structural relaxations, the atomic geometries were fully optimized until the Hellmann–Feynman forces were less than 1 meV/Å. The external electric field was introduced by the planar dipole layer method [43].

3. Results and discussion

3.1. Structural analysis

Ultrathin BTO film was deposited on the (001)-orientated NSTO substrate using L-MBE approach [10,20], and the epitaxial growth is confirmed by XRD data in Fig. 1(a) showing (002) peaks of both BTO and NSTO. RHEED was acquired during deposition for real-time monitoring and control [19,20], as illustrated in Fig. 1(b), and the intensity oscillation of RHEED confirms the high quality layer by layer growth of 7 unit cells BTO. This ultrathin thickness leads to blunt XRD peaks of BTO, as shown in Fig. S1a over a larger range, and RSM around (−103) reciprocal spot in Fig. 1(c) demonstrates that the epitaxial BTO is fully strained on NSTO substrate as no horizontal shift is observed [9,20]. The high quality NSTO/BTO hsterostructure is further examined by cross-sectional HAADF STEM [9,14,23], revealing distinct interface between BTO (left) and NSTO (right) highlighted by colored contrast (Fig. 1(d)). The lattice of epitaxial BTO was mapped *via* IDPC [8,24] in Fig. S1b, exhibiting the ideal structure of Ba, Ti, and O atoms as marked by blue, green and yellow dots. There are no obvious impurities and defects observed in either HAADF or IDPC image, facilitating the subsequent investigation on functional response and polar order of NSTO/BTO heterostructure.

3.2. Apparent piezoresponse reversal

We then applied the widely used PFM [15] to probe possible ferroelectric switching of NSTO/BTO heterostructure. As seen in Fig. S2, the film surface is smooth with root mean square roughness of 175 pm, surface potential of 563±7 mV, and uniform PFM amplitude and phase. After lithography poling *via* the charged probe with 3 V in the inner box and −6 V in the outer box as schematically shown in Fig. S3, opposite PFM phase polarity is observed in the poled region (Fig. 2(a)), wherein PFM amplitude drops at the apparent domain walls (Fig. 2(b)), consistent with supposed 180° polarization reversal in classical ferroelectrics [15]. This opposite polarity is also exhibited by the surface potential contrast (Fig. 2(c)), wherein positively poled region rises to 650 mV and negatively poled region drops to −58 mV. The apparent piezoresponse reversal is further supported by local PFM hysteresis and butterfly loops measured with a relatively soft cantilever of 2.5 N/m under an AC excitation of 1 V (Fig. 2(d)). However, when a stiffer cantilever of 40 N/m was used, the switching characteristics is largely suppressed (Fig. 2(e)). More data on these two different behaviors under different cantilever stiffness are shown in Fig. S4. Similar behavior is observed in nonferroelectric NSTO as well, in sharp contrast with thick ferroelectric BFO film (Fig. S4), suggesting that the observed apparent switching in NSTO/BTO may be caused by artifacts [2,15–17]. Indeed, the contrasts in PFM and surface potential in the poled region are weakened substantially after scanning by a grounded probe, as seen in Fig. 2(f–h) as well as in Figs. S5 and S6, suggesting that either the switched domain is not stable, or the observed contrast is due to mechanisms other than polarization reversal.

To clarify this ambiguity, we examined the nature of observed local piezoresponse in details by comparing the first and second harmonic responses [27,28] averaged over 15 spatial points before and after poling, as well as after grounding, as exhibited in Fig. 2(i–k) with representative raw data in Fig. S7. While the first harmonic piezoresponse dominates the second harmonic one in the virgin state before poling, the trend is reversed after poling regardless of the polarity of the poling voltage. It is interesting that the first harmonic piezoresponse is suppressed substantially after poling, while the magnitude of second harmonic one is not affected much, and the very small data scattering suggests that the trend is highly consistent in different spatial points. This observation casts further doubt on the PFM contrast seen in Fig. 2(ab) as the signature for polarization reversal, since the apparent piezoresponse observed after poling is not linear piezoelectric but exhibits strong nonlinearity. The phenomenon can be understood from the charge injection, which acts as a DC bias and thus does not affect second harmonic piezoresponse. The first harmonic one, however, is suppressed due to charge screening of excitation voltages [27,28]. Indeed, after grounding, the first harmonic response is fully recovered and dominates the second

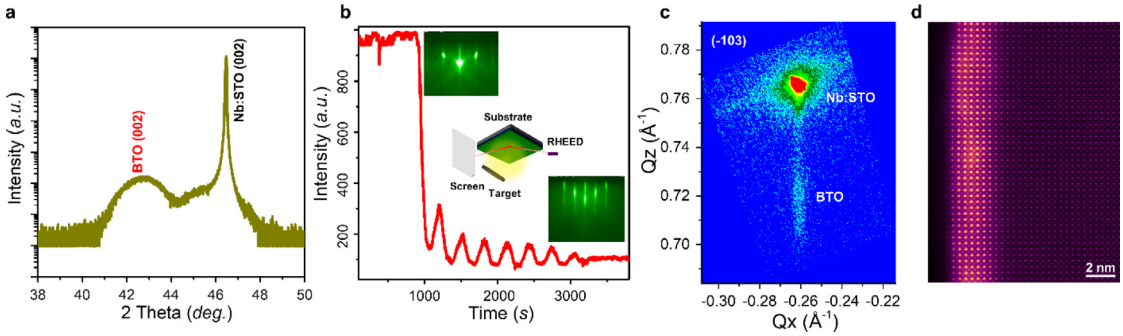

Fig. 1. High quality NSTO/BTO heterostructure deposited by L-MBE; (a) XRD showing (002) peaks for both BTO and NSTO; (b) RHEED confirming the high quality layer by layer growth of 7 unit cells BTO; (c) RSM demonstrating the epitaxial BTO fully strained on NSTO substrate; and (d) cross-sectional HAADF image of NSTO/BTO interface (colored for clarity). (For interpretation of the references to colour in this figure legend, the reader is referred to the web version of this article.)

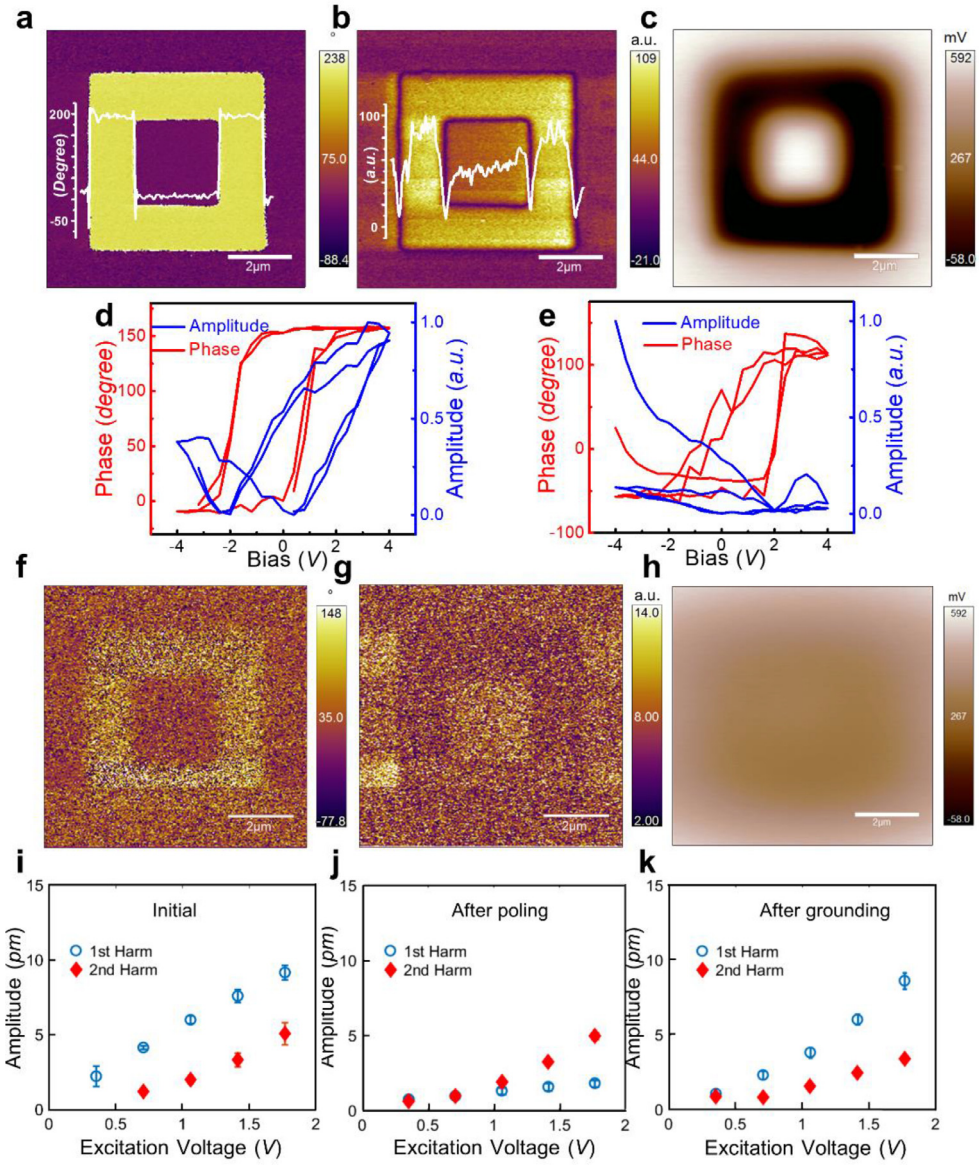

Fig. 2. Piezoresponse and surface potential of NSTO/BTO heterostructure before and after lithography poling, as well as after grounding; (a) PFM phase, (b) amplitude, and (c) KPFM surface potential mappings after poling, imposed by the respective line profiles across the interface; local piezoresponse hysteresis and butterfly loops measured with (d) a soft cantilever of 2.5 N/m and (e) a stiffer cantilever of 40 N/m, under excitation voltage of 1 V; mappings of (f) PFM phase, (g) amplitude, and (h) KPFM surface potential after grounding in the lithographically poled region; and comparisons of first and second harmonic piezoresponses measured with respective to excitation voltage (i) before and (j) after poling, and (k) after grounding. (For interpretation of the references to colour in this figure legend, the reader is referred to the web version of this article.)

harmonic ones, confirming that the observed PFM contrast arises from charge injection instead of polarization reversal. This also explains the suppression of apparent switching behavior by stiffer cantilever seen in Fig. 2(e), because of relatively weak interaction between the probe and surface charges [29].

The charge injection mechanism is further validated by the similar apparent PFM contrast observed in nonferroelectric NSTO substrate after poling (Fig. S8), which vanishes after grounding, as well as the comparison between its first and second harmonic piezoresponses, wherein second harmonic response dominates in NSTO even before poling. True polarization reversal in thick ferroelectric BFO film, on the other hand, clearly shows that the dominance of first harmonic response is maintained after poling (Fig. S9), reflecting its intrinsic linear piezoelectricity with negligible influence of charge injection. The contrasts in PFM and KPFM remain in BFO after grounding as well, in sharp contrast to both NSTO/BTO and NSTO. It is also evident that the written domain wall in BFO is sharp, while that in NSTO/BTO is diffused, consistent with mobile surface charges (Fig. S10), and surface charges on NSTO/BTO also exert significant influences on the contact resonances not seen in BFO. We also increased the temperature of NSTO/BTO to 110 °C after poling to eliminate surface charges while keep it under Curie temperature of bulk BTO [30], and observed substantial drop in PFM contrast during heating (Fig. S11). Similarly, contrasts in PFM and KPFM are smaller in a controlled atmosphere of N_2 compared to ambient (Fig. S12) due to fewer charges available in the environment. In all these processes, no obvious changes in surface topography is observed, excluding possible electrochemical mechanisms for the observed apparent piezoresponse [17]. This set of studies thus unambiguously established the lack of polarization reversal in ultrathin NSTO/BTO heterostructure, even with the presence of weak polar order.

3.3. Atomic-scale polar state

The lack of intrinsic polarization reversal in ultrathin NSTO/BTO heterostructure raises an important question on its possible polar

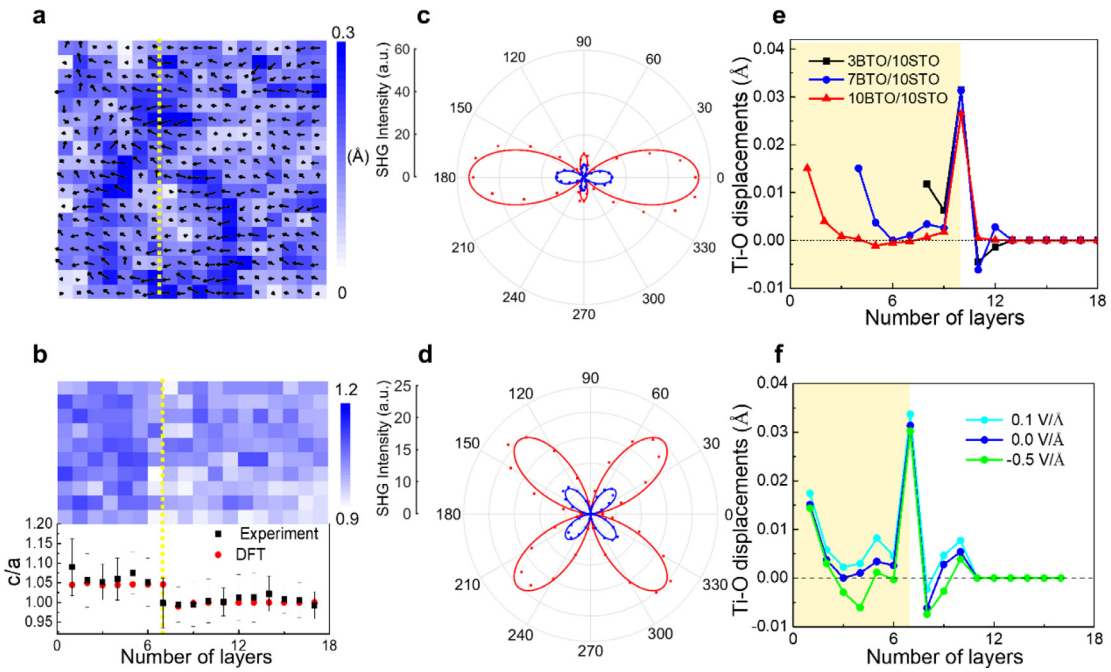

Fig. 3. Atomic-scale polar state of NSTO/BTO heterostructure; (a) distribution of Ti-O displacement derived from IDPC image, wherein the polar displacement vector is overlaid with color mapping representing its magnitude, and the yellow line marks the interface between BTO and NSTO; (b) c/a ratio mapping and comparison of c/a ratio between STEM measurements and DFT calculations; comparisons of (c) P_{out} and (d) S_{out} SHG signals for NSTO/BTO heterostructure (blue, after10 times magnification) and 20 nm BTO (red); (e) profile of Ti-O displacement in STO/BTO heterostructures of different number of BTO unit cells; (f) Ti-O displacement in STO/BTO heterostructure subjected to various electric fields. (For interpretation of the references to colour in this figure legend, the reader is referred to the web version of this article.)

structure, especially given the dominating first harmonic piezoresponse in its virgin state before poling. To shed insight into this question, we examined the Ti-O displacement representing possible polar state of NSTO/BTO at the atomic scale as shown in Fig. 3(a), which is derived from the IDPC image. It is observed that the polar vectors are not aligned, while their magnitudes fluctuate, and there is no obvious difference between BTO and the underlying NSTO substrate. This suggests lack of strong long-range polar orders in 7 u.c. BTO, and the polarization in BTO, if any, is small. Nevertheless, clear distinction in c/a ratio between BTO and NSTO is observed in Fig. 3(b), which agrees well with the DFT calculation, confirming that the 7 u.c. BTO with c/a ratio of approximately 1.05 is indeed tetragonal while the underlying NSTO substrate is cubic. In order to unambiguously establish the long-range polar order in NSTO/BTO, we carried out SHG measurements at macroscopic scale, wherein its SHG intensity is observed to be about two order of magnitude smaller than that of thick BTO film (Fig. 3(cd)), and thus confirm the much reduced polarization in NSTO/BTO. Indeed, such small polarization is supported by first principle calculations based on DFT [31,32]. The calculated Ti-O displacements in STO/BTO heterostructure with 7 u.c. BTO is less than 0.02 Å (Fig. S13), in comparison to ~ 0.12 Å of bulk BTO [33–35]. Similar behavior is also observed in A-O displacement shown. This set of data thus confirm the presence of polar state, albeit weak, in NSTO/BTO heterostructure.

To better understand the effect of BTO thickness of the polar order, we calculate STO/BTO heterostructure with 3, 7, and 10 u.c. of BTO from DFT, as shown in Fig. 3(e), and observe strong surface and interfacial polar state in BTO that is rather insensitive to its thickness. It is believed to be related to the dead layer on the surface and near the interface [8]. The interior polar displacement in 7 u.c. BTO, on the other hand, is rather small, and it increases in 10 u.c. BTO, suggesting polar structure is stabilized in thicker film. We also applied an electric field opposite to the polar direction on the surface of BTO to investigate possible polarization reversal, and observed that the interior polar displacement is not switched until the external electric field approaches −0.5 V/Å (Fig. 3(f)), while the surface polar structure is strongly pinned. This corresponds to approximately an ultrahigh −15 V for the 7 u.c. BTO, while experimental electric breakdown occurs at much smaller voltage. Even under such large electric field, the polar state on the surface is unchanged, consistent with the presence of a dielectric dead layer on the surface. If a small electric field along the direction of the polarization is applied, it is then seen that the polar state is enhanced. Finally, we also analyzed 7 u.c. BTO sandwiched between two $SrRuO_3$ (SRO) electrodes, as shown in Fig. S14, revealing stable polar order from DFT calculations consistent with previous report [35]. This set of study thus shed atomic insight into the irreversibility of polar order in ultrathin STO/BTO heterostructure.

3.4. Resistive switching

Resistive switching in epitaxial BTO/NSTO heterostructures has been widely reported [20,29,36], and the polarization modulated mechanisms has been proposed [12,13,18,19]. It is not clear, however, whether polarization reversal is a prerequisite for the resistive switching in systems with such weak polar order, and how the polar reversibility affect resistive switching performance. To answer these questions, we map local current distribution by conductive AFM (c-AFM) after positive and negative poling, as shown in Fig. 4(a), wherein significant current up to 20 pA is observed in region poled by 3 V, which is much larger than the magnitude measured in region poled by −6 V or without poling (Fig. S15). This is consistent with asymmetric local I-V curves shown in Fig. S15, wherein typical rectifying effect is observed in NSTO/BTO reflecting the resistive switching features with current saturating under different voltages. Interestingly, similar behavior is also observed in bare NSTO substrate, though with smaller asymmetry. As we discussed earlier, such poling process injects surface charges into the film without switching the underlying polarization, suggesting that the polarization reversal is not necessary for resistive switching. In order to firmly establish resistive switching in the system, high work function Pt was deposited as top electrode on NSTO/BTO to conduct macroscopic electric measurements under electric triggering sequence of 0 V→2.5 V→−5 V→0 V, revealing macroscopic resistive switching I-V curve (Fig. S15)

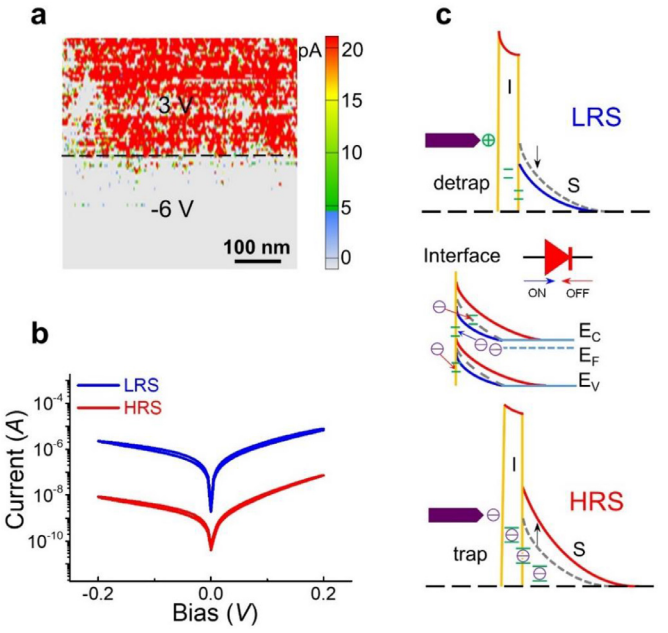

Fig. 4. Resistive switching of NSTO/BTO heterostructure; (a) current mappings in regions poled by 3 V and −6 V; (b) macroscopic I-V curve measured in LRS and HRS states using Pt as top electrode; (c) the proposed resistive switching mechanism with schematic barrier profiles, wherein 'I' stands for interfacial layer and 'S' represents semiconductor layer. (For interpretation of the references to colour in this figure legend, the reader is referred to the web version of this article.)

analogous to microscopic ones. Bi-resistive states can be toggled through adequate positive and negative poling, wherein the high resistive state (HRS) was triggered using −5 V pulse for 5 ms, while 2.5 V pulse for 5 ms was able to convert it to low resistive state (LRS), resulting in I-V curves with distinct current that is 2 orders of magnitude different (Fig. 4(b)). It is generally proposed that such heterostructure is modulated by the ferroelectric layer through polarization switching. Nevertheless, in the absence of the polarization reversal as we demonstrated, such resistive switching still exists and can be understood from charge injection as schematically shown in Fig. 4(c). When negatively (positively) poled tips contact the NSTO/BTO surface, charge trapping (detrapping) occurs, thus lowering (raising) the interface barrier, resulting in LRS (HRS) state [29,37,38]. As such, polarization reversal is not necessary to accomplish resistive switching in a ferroelectric heterostructure, even with the presence of weak polar orders.

4. Conclusion

Unambiguous demonstration of polarization switching is nontrivial even for bulk ferroelectrics [39], and it is even more difficult for ultrathin films. The most direct proof may lies in the in-situ STEM characterization that resolve the atomic scale polar order in real time under electric field [40], though this has yet to be demonstrated in ultrathin films and heterostructures due to a number of technical challenges, to the best of our knowledge. As a result, PFM currently is the tool of choice to assess polarization switching in ferroelectric nanostructures, though cautions must be excised due to possible artifacts involved, not only on the apparent phase contrast [15–17], but also on piezoresponse itself that may not arise from spontaneous polarization [2,27,28]. Our study, however, does not necessarily contradict polarization modulated resistive switching reported earlier [9,12,13,18,19,20,36], as PFM responses were carefully examined in many of these studies, for example, by checking its stability over time [15,18,20], or comparing against reference samples without polarization [29]. What we are learning here is that even in a ferroelectric heterostructure with spontaneous polarization, resistive switching is possible in the absence of polarization reversal due to charge injection. This is similar to that observed in NSTO/Pt heterojunction [37], and can be eliminated by appropriate interface processing [38]. In fact, Liu et al. [29] has suggested that resistive switching in ferroelectric heterostructure may share similar mechanism as that in nonferroelectric NSTO based heterojunction, while we prove that resistive switching can indeed occur in the absence of polarization reversal. It is also important to examine the effect of different thickness of BTO, especially when the polarization switching and charge injection coexist, which we plan to investigate in the future.

Our finding has a number of important technological implications. The ability to (semi-)continuously tune resistance over multiple states is highly desirable for emerging memristor applications such as neuromorphic computing [12,13], and charge injection offers potentially more accessible states than bi-stable polarization modulated mechanism. On the other hand, the presence of spontaneous polarization, even weak, may stabilize one type of the charges injected based on their polarity, an advantage over nonferroelectric NSTO based heterojunction, though the effect of polarization on resistive switching is probably rather minor is this particular system. Finally, the study also raises an important technical challenge to unambiguously demonstrate polarization switching in ultrathin films at their critical size limit. While the existence of polar order in films as thin as 1 u.c. has been firmly established now, confirming its switching at this length scale will open many new exciting possibilities in addition to further shed light into the polar order at this ultimate 2D limit.

Declaration of Competing Interest

The authors declare that they have no known competing financial interests or personal relationships that could have appeared to influence the work reported in this paper.

Acknowledgements

We acknowledge the support of National Key Research and Development Program of China (2016YFA0201001), National Natural Science Foundation of China (11627801, 51702351, 51902337), Shenzhen Science and Technology Innovation Committee (KQTD20170810160424889, JCYJ20170818163, 902553, JCYJ20170413152832151), The Instrument Developing Project of Chinese Academy of Sciences (No. ZDKYYQ20180004) and Key Area R&D Program of Guangdong Province (2018B010109009). P. G. acknowledges the support from the National Natural Science Foundation of China (51672007). We gratefully acknowledge Electron Microscopy Laboratory in Peking University for the use of Cs corrected electron microscope.

Supplementary materials

Supplementary material associated with this article can be found in the online version at doi:10.1016/j.actamat.2020.02.001.

REFERENCES

[1] J.F. Scott, C.A. Paz, de Araujo, Ferroelectric memories, Science 246 (1989) 1400–1405.
[2] R.K. Vasudevan, N. Balke, P. Maksymovych, S. Jesse, S.V. Kalinin, Ferroelectric or non-ferroelectric: why so many materials exhibit "ferroelectricity" on the nanoscale, Appl. Phys. Rev 4 (2017) 021302.
[3] J. Junquera, P. Ghosez, Critical thickness for ferroelectricity in perovskite ultrathin films, Nature 422 (2003) 506–509.
[4] W.L. Zhong, Y.G. Wang, P.L. Zhang, B.D. Qu, Phenomenological study of the size effect on phase transitions in ferroelectric particles, Phys. Rev. B Condens. Matter 50 (1994) 698–703.
[5] Y.J. Shin, Y. Kim, S.J. Kang, H.H. Nahm, P. Murugavel, J.R. Kim, M.R. Cho, L. Wang, S.M. Yang, J.G. Yoon, J.S. Chung, M. Kim, H. Zhou, S.H. Chang, T.W. Noh, Interface control of ferroelectricity in an $SrRuO_3$/$BaTiO_3$ /$SrRuO_3$ capacitor and its critical thickness, Adv. Mater. 29 (2017) 1602795.
[6] S.R. Lee, L. Baasandorj, J.W. Chang, I.W. Hwang, J.R. Kim, J.G. Kim, K.T. Ko, S.B. Shim, M.W. Choi, M. You, C.H. Yang, J. Kim, J. Song, First observation of

ferroelectricity in approximately 1 nm ultrathin semiconducting $BaTiO_3$ films, Nano Lett. 19 (2019) 2243–2250.
[7] G. Gerra, A.K. Tagantsev, N. Setter, K. Parlinski, Ionic polarizability of conductive metal oxides and critical thickness for ferroelectricity in $BaTiO_3$BaTiO, Phys. Rev. Lett. 96 (2006) 107603.
[8] P. Gao, Z. Zhang, M. Li, R. Ishikawa, B. Feng, H.J. Liu, Y.L. Huang, N. Shibata, X. Ma, S. Chen, J. Zhang, K. Liu, E.G. Wang, D. Yu, L. Liao, Y.H. Chu, Y. Ikuhara, Possible absence of critical thickness and size effect in ultrathin perovskite ferroelectric films, Nat. Commun. 8 (2017) 15549.
[9] H. Wang, H. Wang, Z.R. Liu, H.Y. Yoong, T.R. Paudel, J.X. Xiao, R. Guo, W.N. Lin, P. Yang, J. Wang, G.M. Chow, T. Venkatesan, E.Y. Tsymbal, H. Tian, J.S. Chen, Direct observation of room-temperature out-of-plane ferroelectricity and tunneling electroresistance at the two-dimensional limit, Nat. Commun. 9 (2018) 3319.
[10] D. Ji, S. Cai, T.R. Paudel, H. Sun, C. Zhang, L. Han, Y. Wei, Y. Zang, M. Gu, Y. Zhang, W. Gao, H. Huyan, W. Guo, D. Wu, Z. Gu, E.Y. Tsymbal, P. Wang, Y. Nie, X. Pan, Freestanding crystalline oxide perovskites down to the monolayer limit, Nature 570 (2019) 87–90.
[11] L. Wang, Q. Feng, Y. Kim, R. Kim, K.H. Lee, S.D. Pollard, Y.J. Shin, H. Zhou, W. Peng, D. Lee, W. Meng, H. Yang, J.H. Han, M. Kim, Q. Lu, T.W. Noh, Ferroelectrically tunable magnetic skyrmions in ultrathin oxide heterostructures, Nat. Mater. 17 (2018) 1087–1094.
[12] V. Garcia, M. Bibes, Ferroelectric tunnel junctions for information storage and processing, Nat. Commun. 5 (2014) 4289.
[13] L.W. Martin, A.M. Rappe, Thin-film ferroelectric materials and their applications, Nat. Rev. Mater. 2 (2016) 16087.
[14] M.J. Polking, M.G. Han, A. Yourdkhani, V. Petkov, C.F. Kisielowski, V.V. Volko, Y. Zhu, G. Caruntu, A.P. Alivisatos, R. Ramesh, Ferroelectric order in individual nanometre-scale crystals, Nat. Mater. 11 (2012) 700–709.
[15] A. Gruverman, M. Alexe, D. Meier, Piezoresponse force microscopy and nanoferroic phenomena, Nat. Commun. 10 (2019) 1661.
[16] N. Balke, P. Maksymovych, S. Jesse, A. Herklotz, A. Tselev, C.B. Eom, I.I. Kravchenko, P. Yu, S.V. Kalinin, Differentiating ferroelectric and nonferroelectric electromechanical effects with scanning probe microscopy, ACS Nano 9 (2015) 6484–6492.
[17] S.V. Kalinin, Y. Kim, D.D. Fong, A.N. Morozovska, Surface-screening mechanisms in ferroelectric thin films and their effect on polarization dynamics and domain structures, Rep. Prog. Phys. 81 (2018) 036502.
[18] V. Garcia, S. Fusil, K. Bouzehouane, S. Enouz-Vedrenne, N.D. Mathur, A. Barthelemy, M. Bibes, Giant tunnel electroresistance for non-destructive readout of ferroelectric states, Nature 460 (2009) 81–84.
[19] A. Gruverman, D. Wu, H. Lu, Y. Wang, H.W. Jang, C.M. Folkman, M.Y. Zhuravlev, D. Felker, M. Rzchowski, C.B. Eom, E.Y. Tsymbal, Tunneling electroresistance effect in ferroelectric tunnel junctions at the nanoscale, Nano Lett 9 (2009) 3539–3543.
[20] Z. Wen, C. Li, D. Wu, A.D. Li, N.B. Ming, Ferroelectric-field-effect-enhanced electroresistance in metal/ferroelectric/semiconductor tunnel junctions, Nat. Mater. 12 (2013) 617–621.
[21] L.F. Wang, R. Kim, Y. Kim, C.H. Kim, S. Hwang, M.R. Cho, Y.J. Shin, S. Das, J.R. Kim, S.V. Kalinin, M. Kim, S.M. Yang, T.W. Noh, Electronic-reconstruction-enhanced tunneling conductance at terrace edges of ultrathin oxide films, Adv. Mater. 29 (2017) 1702001.
[22] J.W. Hu, Z.H. Wang, W.L. Yu, T. Wu, Optically controlled electroresistance and electrically controlled photovoltage in ferroelectric tunnel junctions, Nat. Commun. 7 (2016) 10808.
[23] S. Zhang, X. Guo, Y. Tang, D. Ma, Y. Zhu, Y. Wang, S. Li, M. Han, D. Chen, J. Ma, B. Wu, X. Ma, Polarization rotation in ultrathin ferroelectrics tailored by interfacial oxygen octahedral coupling, ACS Nano 12 (2018) 3681–3688.
[24] P. Gao, H.J. Liu, Y.L. Huang, Y.H. Chu, R. Ishikawa, B. Feng, Y. Jiang, N. Shibata, E.G. Wang, Y. Ikuhara, Atomic mechanism of polarization-controlled surface reconstruction in ferroelectric thin films, Nat. Commun. 7 (2016) 11318.
[25] M. Trassin, G.D. Luca, S. Manz, M. Fiebig, Probing ferroelectric domain engineering in $BiFeO_3$ thin films by second harmonic generation, Adv. Mater. 27 (2015) 4871–4876.
[26] Y. Zhang, Y. Zhang, Q. Guo, X.G. Zhong, Y.H. Chu, H.D. Lu, G.K. Zhong, J. Jiang, C.B. Tan, M. Liao, Z.H. Lu, D.W. Zhang, J.B. Wang, J.M. Yuan, Y.C. Zhou, Characterization of domain distributions by second harmonic generation in ferroelectrics, npj Comput. Mater 4 (2018) 39.
[27] Q.N. Chen, Y. Ou, F.Y. Ma, J.Y. Li, Mechanisms of electromechanical coupling in strain based scanning probe microscopy, Appl. Phys. Lett. 104 (2014) 242907.
[28] J.Y. Li, J.-F. Li, Q. Yu, Q.N. Chen, S.H. Xie, Strain-based scanning probe microscopies for functional materials, biological structures, and electrochemical systems, J. Materiomics 1 (2015) 3–21.
[29] Z. Fan, H. Fan, L. Yang, P.L. Li, Z.X. Lu, G. Tian, Z.F. Huang, Z.W. Li, J.X. Yao, Q.Y. Luo, C. Chen, D.Y. Chen, Z.B. Yan, M. Zeng, X.B. Lu, X.S. Gao, J.-M. Liu, Resistive switching induced by charge trapping/detrapping: a unified mechanism for colossal electroresistance in certain Nb:$SrTiO_3$-based heterojunctions, J. Mater. Chem. C 5 (2017) 7317–7327.
[30] G.H. Kwei, A.C. Lawson, S.J.L. Billinge, S.-W. Cheong, Structures of the ferroelectric phases of Barium-Titanate, J. Phys. Chem-Us 97 (1993) 2368–2377.
[31] P. Hohenberg, W. Kohn, Inhomogeneous electron gas, Phys. Rev. 136 (1964) B864–B871.
[32] W. Kohn, L.J. Sham, Self-consistent equations including exchange and correlation effects, Phys. Rev 140 (1965) A1133–A1138.
[33] M.B. Smith, K. Page, T. Siegrist, P.L. Redmond, E.C. Walter, R. Seshadri, L.E. Brus, M.L. Steigerwald, Crystal structure and the paraelectric-to-ferroelectric phase transition of nanoscale $BaTiO_3$BaTiO, J. Am. Chem. Soc. 130 (2008) 6955–6963.
[34] C.G. Duan, S.S. Jaswal, E.Y. Tsymbal, Predicted magnetoelectric effect in Fe/$BaTiO_3$ multilayers: ferroelectric control of magnetism, Phys. Rev. Lett. 97 (2006) 047201.
[35] J.P. Velev, C.G. Duan, J.D. Burton, A. Smogunov, M.K. Niranjan, E. Tosatti, S.S. Jaswal, E.Y. Tsymbal, Magnetic tunnel junctions with ferroelectric barriers: prediction of four resistance states from first principles, Nano Lett 9 (2009) 427–432.
[36] Z. Xi, J. Ruan, C. Li, C. Zheng, Z. Wen, J. Dai, A. Li, D. Wu, Giant tunnelling electroresistance in metal/ferroelectric/semiconductor tunnel junctions by engineering the schottky barrier, Nat. Commun. 8 (2017) 15217.
[37] D. Kan, Y. Shimakawa, Transient behavior in Pt/Nb-doped $SrTiO_3$ schottky junctions, Appl. Phys. Lett. 103 (2013) 142910.
[38] E. Mikheev, B.D. Hoskins, D.B. Strukov, S. Stemmer, Resistive switching and its suppression in Pt/Nb:$SrTiO_3$ junctions, Nat. Commun. 5 (2014) 3990.
[39] J.F. Scott, Ferroelectrics go bananas, J. Phys. Condens. Matter 20 (2008) 021001.
[40] C.T. Nelson, P. Gao, J.R. Jokisaari, C. Heikes, C. Adamo, A. Melville, S.H. Baek, C.F. Folkman, B. Winchester, Y. Gu, Y. Liu, K. Zhang, E. Wang, J. Li, L.Q. Chen, C.B. Eom, D.G. Schlom, X. Pan, Domain dynamics during ferroelectric switching, Science 334 (2011) 968–971.
[41] P.E. Blochl, O. Jepsen, O.K. Andersen, Improved tetrahedron method for Brillouin-Zone integrations, Phys. Rev. B Condens. Matter 49 (1994) 16223–16233.
[42] G. Kresse, D. Joubert, From ultrasoft pseudopotentials to the projector augmented-wave method, Phys. Rev. B 59 (1999) 1758–1775.
[43] J. Neugebauer, M. Scheffler, Adsorbate-substrate and adsorbate-adsorbate interactions of Na and K adlayers on Al (111), Phys. Rev. B 46 (1992) 16067–16080.